Dynamics of transition metal dissolution and cross-contamination in operating Lithium-ion batteries

Antonin Gajan, Kethsovann Var, Rajmohan Rajendiran, Jean-François Lemineur, Olivier Guiader, Benoit Mortemard de Boisse, Bernard Simon, Julien Demeaux, Ivan Lucas

Journal of Power Sources 630 (2025) 236031

Contents lists available at ScienceDirect

Journal of Power Sources

journal homepage: www.elsevier.com/locate/jpowsour

Dynamics of transition metal dissolution and cross-contamination in operating Lithium-ion batteries

Antonin Gajan [a,d], Kethsovann Var [a], Rajmohan Rajendiran [b], Jean-François Lemineur [c], Olivier Guiader [d], Benoit Mortemard de Boisse [d], Bernard Simon [d], Julien Demeaux [d], Ivan T. Lucas [a,b,1,*]

[a] Sorbonne Université, CNRS, Laboratoire Interfaces et Systèmes électrochimiques, LISE, UMR 8235, F-75000, Paris, France
[b] Nantes Université, CNRS, Institut des Matériaux de Nantes Jean Rouxel, IMN, UMR 6502, F-44000, Nantes, France
[c] Paris Cité Université, CNRS, Laboratoire Interfaces Traitements Organisation et Dynamique des Systèmes, ITODYS, UMR7086, 75013, Paris, France
[d] Saft, Corporate Research, F-33074, Bordeaux, France

HIGHLIGHTS

- Simple operando crosstalk sensor with minimal electrochemical "footprint".
- Real-time tracking and trapping of redox shuttles by electrodeposition.
- Quantification of LNMO dissolution at any operating voltage.
- Larger dissolution at high voltages and in less oxidation resistant electrolytes.

GRAPHICAL ABSTRACT

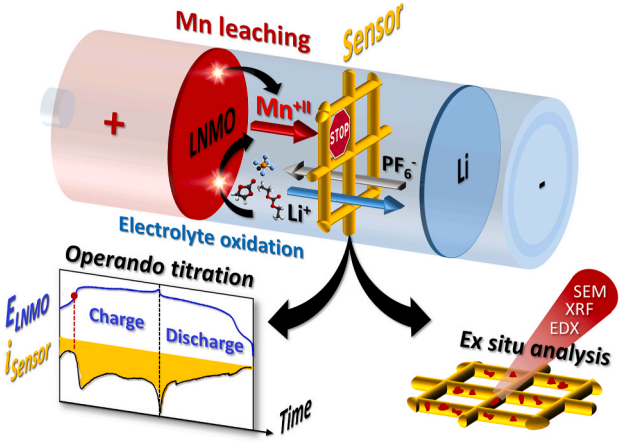

ARTICLE INFO

Keywords:
Redox shuttle
Crosstalk
Operando
Real-time detection
LNMO
High-voltage cathode

ABSTRACT

Chemical crosstalk in functioning batteries, which describes the shuttling of electrolyte soluble reactive species through the separator and the disruption of the electrode operation is a major concern, which impacts the development of new electrode generation for lithium or sodium ion/metal batteries and therefore needs to be addressed urgently. The accurate depiction of the origin, the dynamics and deleterious effects of crosstalk process upon cycling of the battery, precondition to possible remediation, requires new operando diagnostic solutions. In this work, a powerful crosstalk sensing technique based on the electrochemical trapping of redox shuttles is introduced and applied to the high-voltage $LiNi_{0.5}Mn_{1.5}O_4$ (LNMO) cathode material. Leaching and transport of

* Corresponding author. Nantes Université, CNRS, Institut des Matériaux de Nantes Jean Rouxel, IMN, UMR 6502, F-44000, Nantes, France
E-mail address: ivan.lucas@cnrs-imn.fr (I.T. Lucas).
[1] Lead Contact.

https://doi.org/10.1016/j.jpowsour.2024.236031
Received 7 September 2024; Received in revised form 2 December 2024; Accepted 5 December 2024
Available online 17 December 2024

transition metal species from the LNMO composite electrode and of electrolyte oxidation products could be evidenced, quantified and tracked upon cycling of the LNMO//Li system, unraveling the critical impact of the electrolyte composition and its resistance to oxidation.

1. Introduction

Operando diagnostic techniques that allow real-time monitoring of the battery during operation can facilitate the deconvolution of entangled processes (usually difficult with ex situ analyses), and speed up the search for remediation. The development of such tools that operate under conditions as close as possible to those of functional battery cells and that offer a trade-off between cumbersome/costly implementation and powerful analytical resolution is the subject of intense research efforts. In this work, we propose a rather simple sensing technique to monitor and capture in real time redox-active "shuttles" intercrossing between the positive and negative electrodes in high-energy Li-ion batteries (LIBs), as an alternative to operando techniques like X-ray absorption (XAS) [1,2] and magnetic nuclear resonance (NMR) spectroscopies [3].

The so-called chemical crosstalk effect, which is believed to be detrimental to the battery operation, has been evidenced in batteries using positive electrode materials based on transition metal oxides or phosphates and with spinel (such as $LiMn_2O_4$, LMO), layered ($LiCoO_2$, LCO) or olivine ($LiFePO_4$, LFP) structures. The incriminated redox-active "shuttles" originates from leaching of transition metals from the host materials [4–12] and but also from pronounced oxidation of LIB electrolytes on the material surface at high-operating voltage [13–15] and strongly contribute to the battery capacity fading. Contamination [6,16–27] of the Solid Electrolyte Interphase (SEI) at the negative electrode by metallic species is suspected to either create electronically conductive pathway within the SEI [18,21], to disrupt the SEI passivating ability (porous SEI formation) [18] or to promote its decomposition (e.g. of LEDC) [17,28]. Meanwhile, species produced at the anode, i.e. gas but also electrolyte degradation by-products (organophosphates)' [29], have been reported to be detrimental to the cathode operation (growth of high impedance surface film and loss of active material). The accurate depiction of the origin, dynamics, magnitude and deleterious effects of crosstalk process during cycling of the battery, as a prerequisite for possible remediation, requires new diagnostic solutions.

Various in situ/operando spectroscopic techniques have been developed to track and/or identify in situ/operando, the formation of (i) gases [30–32] (online electrochemical mass spectroscopy OEMS [25]), (ii) of electrolyte-soluble metallic and non-metallic species (nuclear magnetic resonance NMR, electron paramagnetic EPR [3], and UV–vis spectroscopy [33]) and (iii) the accumulation of metallic species at the negative (X-Ray absorption spectroscopy XAS [1,2]) or positive electrode (labelled and label-free fluorescence microspectrometry [34,35]). "Generator–collector" electrochemical techniques have been also proposed to register the electrochemical signature (i.e. cyclic voltammetry) of metallic but also non-metallic species intercrossing between the positive and negative electrodes [36,37], though on model systems. The so-called four-electrode techniques include Scanning Electrochemical Microscopy SECM [38], Rotating Ring-Disk Electrode RRDE [39], Li/Pt sense cell [40] inserted at the edge of the separator of a graphite/Li cell and Li|C-Al_2O_3|C-Al_2O_3| Li symmetrical cell [41]. More recently, advanced electrochemical testing protocols have been also proposed to detect crosstalk effects upon aging of the battery and quantify their impact on the battery lifetime [39].

Our new approach for operando crosstalk sensing introduces within the electrode assembly a polarized platinum mesh (sensor), so that redox active oxidation products generated at the positive electrode upon charging and diffusing/migrating toward the negative electrode, i.e. redox shuttles, can be reduced and potentially trapped by electroplating, while avoiding electrolyte reduction. The use of a metal mesh in between the positive and negative electrode in alternative to small surface electrodes classically used for analytical electrochemistry (disc, sphere), gives access to higher sensitivity, reproducibility (direct positioning across the process) and possible quantification of dissolved metal (operando crosstalk sensing/"titration" and ex situ X-ray fluorescence XRF measurements on the Pt mesh), while maintaining the electrochemical performance of the cell.

The proposed methodology was applied to the dynamic quantification of the dissolution extent of the $LiNi_{0.5}Mn_{1.5}O_4$ (LNMO) spinel material upon cycling of the LNMO/Li system in Swagelok cells. In LNMO ($LiNi^{+\,II}_{0.5}Mn^{+\,IV}_{1.5}O_4$), the nickel-doped analogue of LMO ($LiMn^{+\,III}Mn^{+\,IV}O_4$), Mn has been partially substituted by Ni in order to reduce the $Mn^{+\,III}$ content (subject to Jahn-Teller distortion and Hunter disproportionation reactions producing soluble $Mn^{+\,IV}$ and $Mn^{+\,II}$ [38,42]), while significantly increasing the working voltage and thus, the associated energy. Still, significant dissolution of the active material has been evidenced (mainly Mn but also Ni) [19,23]. The mechanism and dynamics of dissolution upon cycling of transition metal oxides including LNMO remains a matter of debate within the scientific community, various degradation schemes being already proposed: (i) disproportionation reactions enhanced in the discharge state (i.e. in the lower valence states of Mn), (ii) phase transformation (as an alternative or additional to disproportionation) with concomitant release of oxygen and soluble metal species) [43,44], (iii) surface catalytic reaction of the high-valence Mn species ($Mn^{+\,IV}$) with electrolyte [19,45] and formation of stables complexes between molecular chelation agents (ligands as oxalate, carbonate, ethylene dicarbonate [46], β-diketonate [23]) and Mn species, promoting Mn dissolution. Note that material corrosion by HF promoted at elevated temperature leading to surface deposits or to soluble metal species [47–49] (decomposition of PF_6^- into F^- and oxidation of alkoxides, semi-carbonates …) has been also reported. To get a better understanding of the intricate dissolution mechanism explaining the capacity fading of LNMO-based systems in operation, the impact of the electrolyte composition and of the $Mn^{+\,III}$ content (disordered or partially ordered LNMO structure) was assessed using our newly developed crosstalk sensing method.

2. Material and methods

LNMO composite electrodes - LNMO powder ("disordered") was synthesized in SAFT adapting protocols detailed by Aktekin et al. [50]. LNMO powder, with lower $Mn^{+\,III}$ content ("partially-ordered") was obtained after a heat treatment of 12 h at 600 °C under a constant flow of oxygen (see Fig. S1). Composite LNMO electrodes (LNMO powder, carbon black, PVDF binder, mass loading 7 mg cm^{-2}) were prepared on aluminum current collectors by SAFT (the nature of the carbon black, binder, proportions and porosity cannot be disclosed). LNMO electrode and lithium negative electrode were assembled in a coin-cell (2032 format) filled with either electrolyte mixtures (volume 20 μL) of ethylene carbonate (EC) and ethyl methyl carbonate (EMC) EC/EMC (30/70: v/v) with 1.2 M $LiPF_6$ or of EC and diethyl carbonate (DEC) EC/DEC (50/50: v/v) with 1.0 M $LiPF_6$ (Solvionic, France) and cycled galvanostatically at a C/10 C-rate (see full description in SI).

Cross-talk sensing method description - The proposed configuration enabling detection and trapping of diffusing species upon charging/discharging of the battery is depicted in Fig. 1a and b and Fig. S2.

A platinum electrode (circular mesh: 13 mm-diameter, 60 μm-thickness, 300 μm-mesh size), is inserted between the positive and negative electrode through the vertical opening of a T-shape Swagelok© type cell, and electrically insulated from the positive and negative

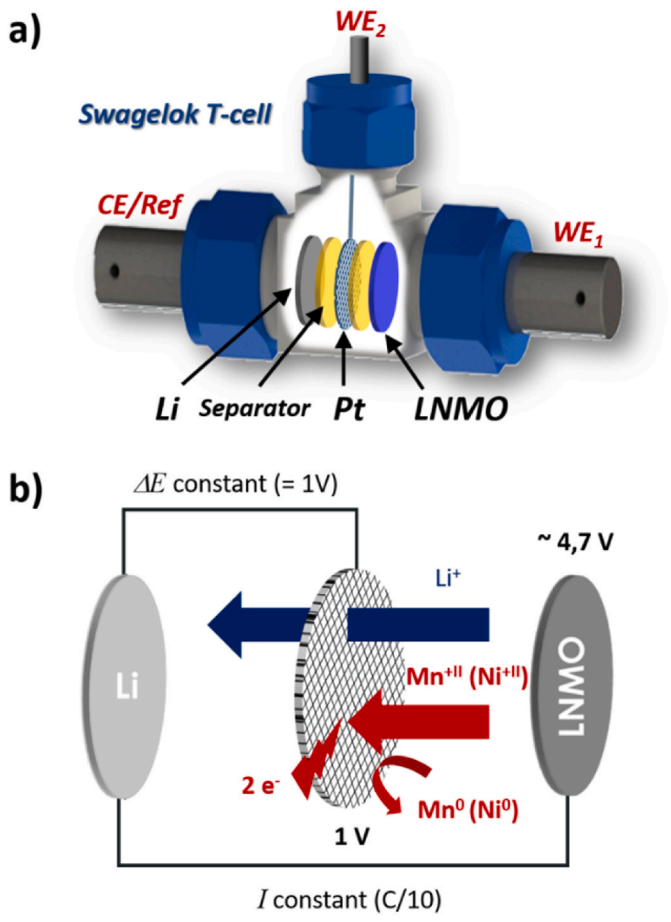

Fig. 1. Crosstalk sensor - a) Experimental set-up: the two working electrodes, LNMO (WE_1) and the Pt grid (WE_2, electrically insulated with polypropylene separators), and the counter-electrode (a Li foil) are assembled in a T-shape Swagelok cell and connected to a bipotentiostat (two Origalys "Origaflex" potentiostat modules sharing the same ref/counter electrodes); **b) Concept**: a polarized Pt mesh (constant voltage: 1 V vs Li/Li^+) is positioned between the two electrodes of a LNMO/Li system to detect and trap transition metals (Mn, Ni …) leaching from the positive electrode and migrating toward the negative electrode upon cycling of the battery (galvanostatic charging at C/10 rate).

electrodes using 2 x 2 polypropylene separators. The Swagelok cell is then filled with LIB electrolytes (volume: 120 µL), sealed and connected to a multi-channel potentiostat (Origaflex, Origalys, France). To ensure that the transition metal-derived compounds leaching from the positive electrodes (Mn, Ni elemental or complex species) could be electroreduced on Pt while minimizing possible concomitant electroreduction of the electrolyte (side reactions), a constant polarization at 1 V vs Li/Li^+ was selected. This latter stands well below the standard reduction potential of Mn/Mn^{2+} and Ni/Ni^{2+} (+1.27 V and +2.22 V vs Li/Li^+ respectively [2]) and above the reduction threshold of the EC-EMC $LiPF_6$ electrolyte (~0.8 V vs Li/Li^+ on Pt [51]). The evaluation of the background current at 1V can be found in Fig. S3 as well as the influence of the LNMO polarization on the sensor response in Fig. S4. All electrochemical experiments were conducted at room temperature.

Post-mortem analyses - After disassembly of the Swagelok© T-cells, Energy dispersive X-Ray spectroscopy (SEM-EDX, ULTRA 55, ZEISS) and X-Ray fluorescence (WDXRF Zetium, Malvern Panalytical) measurements were conducted on the Pt sensor, previously rinsed with EMC electrolyte (see Figs. S13 and S14).

3. Results and discussion

1 Crosstalk sensing on operating LNMO

The cycling performance of LNMO composite electrode vs Li in the modified Swagelok cell with the Pt sensor were first evaluated and compared to the one obtained in LNMO/Li coin-cells (EC/EMC 1.2 M $LiPF_6$ electrolyte, C-rate: C/10). Similar voltage profile and capacity were obtained despite the presence of the 100 µm-thick platinum mesh and of the 2 x 2 polypropylene separators (see Fig. S9). Crosstalk evaluation was then carried out on the (+)LNMO||(Pt_{Sensor})||Li(−) system upon multiple charging/discharging cycles at C/10. The potential profile of LNMO associated to the first cycle and the reduction current obtained in parallel on the platinum mesh sensor (biased at 1V vs Li/Li^+) are shown on Fig. 2a (the 5 successive cycles are displayed in Fig. 4a).

The platinum sensor response shows fluctuating reduction current intensities, which can be attributed to various dissolution regimes of the LNMO electrode convoluted by mass transport process to the sensor. Four main sections during each charge/discharge cycle of the LNMO/Li system can be identified: (i) a first intense reduction current peak (~−3.5 µA) at the beginning of the charge concomitant with the oxidation step at E > 4 V on the potential profile ($Mn^{+\ III/IV}$ to $Ni^{+\ II/III}$ transition) which could be associated to a LNMO structure change promoting its dissolution, (ii) a relaxation at E > 4.5 V to an almost constant current at mid-charge (~−2.1 µA), with a slight variation across the second oxidation step on the potential profile ($Ni^{+\ II/III}$ to $Ni^{+\ II/IV}$ transition) which could suggest a continuous active material dissolution, though at lower rate, concomitant with the electrolyte oxidation, (iii) a marked increase in the reduction current at the end of the charge up to −4.5 µA which could result from the faster migration at high voltages of accumulated charge species at the electrode/electrolyte interface, and (iv) a current which decreases initially fast then steadily down to 0 during the discharge. This apparently lower dissolution rate upon discharge, i.e. where Mn is expected to return to its + III valence state, does not support a dissolution mechanism based (solely) on a disproportionation reaction. Note that the overall reduction current intensity (and the associated charge on Fig. S10b) decreases slightly over the 5 cycles as can be seen in Fig. 4a, suggesting that the dissolution process becomes less and less pronounced upon cycling.

To push further the analysis, the Mn leaching extent at the different operating stages of LNMO during the first LNMO charge and discharge was then evaluated from incremental capacity curves (dQ/dE vs E_{LNMO}) plotted for both electrodes (LNMO and sensor) on Fig. 3. The apparent synchronicity between the dissolution process and the detection at the sensor is striking, the dissolution extent appears higher upon the $Ni^{2+/3+}$ and $Ni^{3+/4+}$ voltage plateaus, despite the apparent faster rate (higher peak current) observed at the $Mn^{3+/4+}$ stage. To confirm this trend, the charges measured at the sensor at the different LNMO operation stages were normalized by the respective amount of Mn and Ni in the electrode. The ratio of charge at the sensor and at the LNMO electrode, deduced from the area below each peak measured at each voltage plateau (yellow: $Mn^{3+/4+}$, red: $Ni^{2+/3+}$ and blue: $Ni^{3+/4+}$) are gathered in Table 1. The higher ratios (factor 2) determined during the $Ni^{2+/3+}$ and $Ni^{3+/4+}$ reactions as compared to $Mn^{3+/4+}$ suggest that Mn dissolution/transport is more pronounced at higher potentials, where electrolyte oxidation is expected to take place concomitantly, and more pronounced during charging compared to discharging. These results are consistent with the sharp increase in fluorescence signal intensity at the threshold of the Ni^{2+} oxidation reaction and the slow decrease upon discharge, as reported by Norberg et al. [34] during operando fluorescence measurements on LNMO/Li.

2 Post-mortem analyses of the sensor

Following cycling, the 3-electrode Swagelok cell was dismounted, the Pt sensor rinsed with EMC and analyzed by SEM-EDX. For

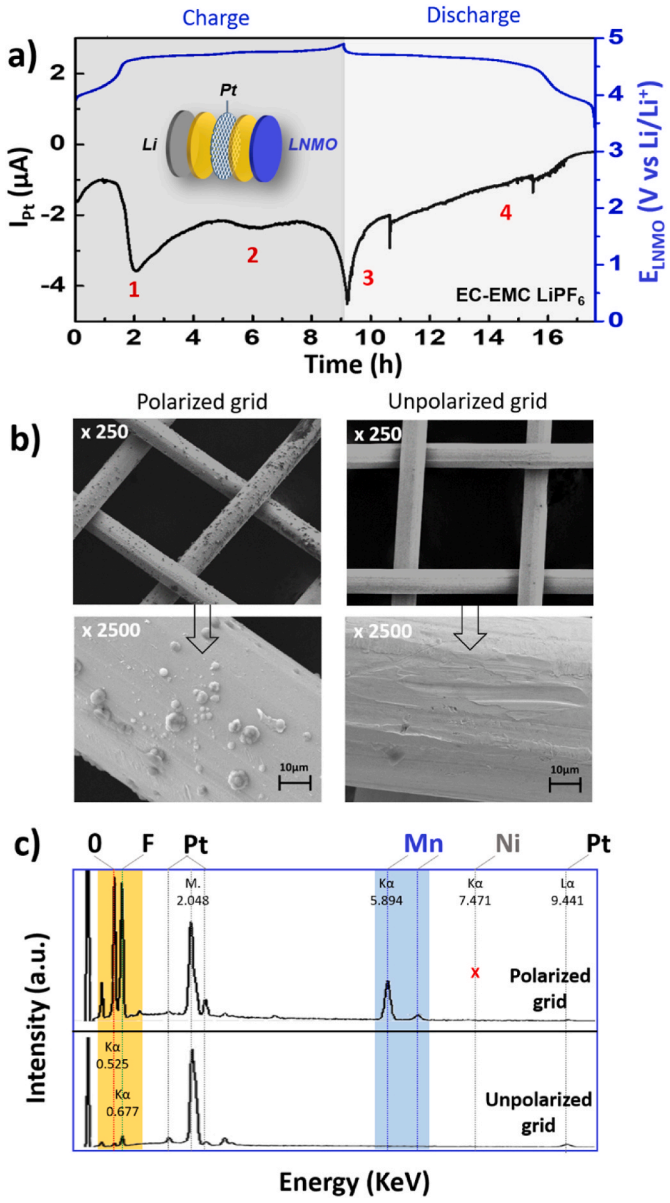

Fig. 2. Crosstalk sensing on the operating LNMO/Li system - a) Potential profile of disordered LNMO upon charging and discharging at C/10 of the LNMO||(Pt_{Sensor})||Li T-shape Swagelok cell in 1.2 M $LiPF_6$ in EC/EMC = 30/70 (v/v) electrolyte (first cycle, in blue) and reduction current measured at the platinum grid sensor biased at 1 V vs Li/Li^+ (chronoamperometry, in black); **b)** SEM post-mortem analysis of the biased platinum mesh evidencing surface deposits as compared to the non-polarized (OCV) mesh and **c)** associated EDX analyses revealing Mn, O, F in addition to Pt. The Pt meshes were disassembled and rinsed prior to their analysis. (For interpretation of the references to color in this figure legend, the reader is referred to the Web version of this article.)

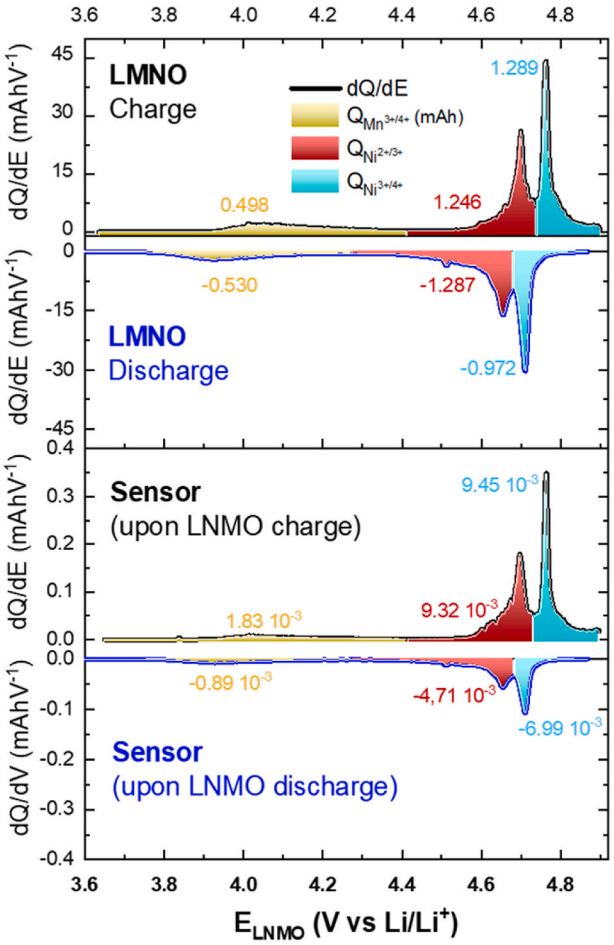

Fig. 3. Incremental capacity curves (dQ/dE) – Top: measured at the LNMO electrode (1st charge and 1st discharge), **bottom:** measured at the Pt sensor. The integrated areas enlightened in color correspond to the charge measured at the LNMO electrode and at the sensor at each operating stage of the LNMO electrode ($Mn^{3+/4+}$, $Ni^{2+/3+}$, $Ni^{3+/4+}$ reactions associated to voltage plateaus of the LNMO charge/discharge curves shown in Fig. 3a). The associated charge values (in mAh) are indicated using the same color code. Note that the absolute value of the charge at the sensor (which is always negative) has been reported during the LNMO charge for ease of comparison. Charge and discharge of the LNMO||(Pt_{Sensor})||Li T-shape Swagelok cell were achieved at a C/10 C-rate in 1.2 M $LiPF_6$ in EC/EMC = 30/70 (v/v) electrolyte. (For interpretation of the references to color in this figure legend, the reader is referred to the Web version of this article.)

comparison, post-mortem analyses were also carried out on a Pt mesh that was kept at the Open Circuit Voltage OCV (not polarized at 1 V) upon cycling of a second LNMO||(Pt_{Sensor})||Li cell. Heterogeneous surface deposits are clearly evidenced on the 1V-biased Pt mesh as shows on the SEM micrograph presented on Fig. 2b, and are associated to high concentration of Mn together with O and F (see EDX data on Fig. 2c). These latter can be associated to electrodeposition of redox shuttles originating from electrolyte oxidation as described earlier on carbon and most likely to electroreduction/deposition of complex manganese species with their chelating agents. The absence of Mn deposits on the Pt sensor maintained at the OCV suggests that Mn species generated upon cycling do not deposit spontaneously on the non-polarized platinum surface. Small amounts of F and O detected on the non-polarized Pt grid could correspond to residues of electrolyte after rinsing and/or to electrolyte degradation products on Pt.

3 Toward quantification: crosstalk sensing on model manganese, copper, and carbon systems

As the proposed configuration enabling trapping of diffusing species upon charging/discharging of the battery is not common, the relevance of the proposed methodology was therefore first assessed through a series of preliminary tests carried out on model systems (see full description in SI).

- The Mn capture efficiency was first assessed using a pure manganese foil as positive electrode on a Mn||(Pt_{Sensor})||Li cell filled with EC/EMC (30/70: v/v) 1.2 M $LiPF_6$ electrolyte. The detection of dissolved manganese turned out to be successful with an estimated “capture

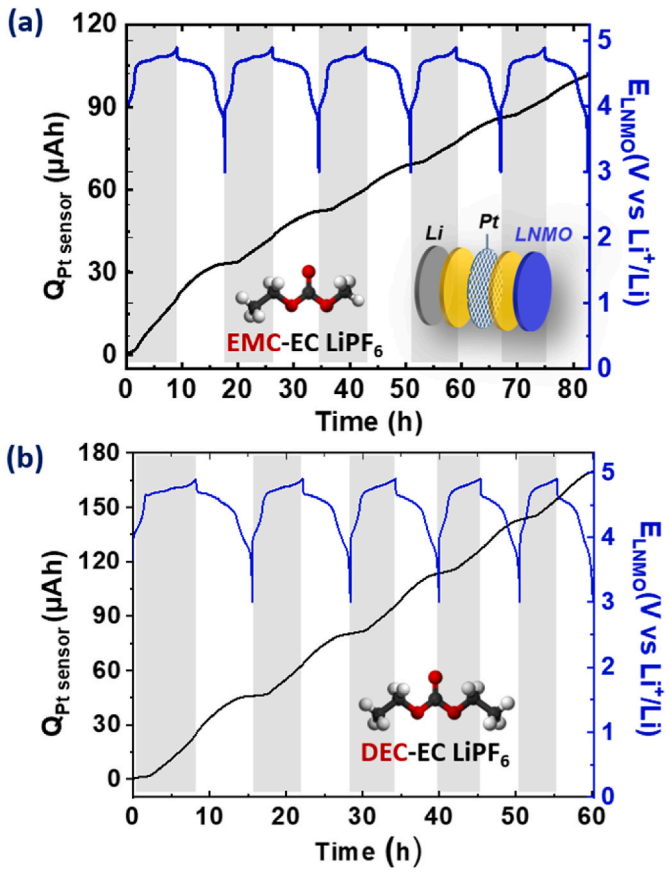

Fig. 4. Impact of the electrolyte composition – Crosstalk sensing experiments carried out on the LNMO||(Pt_{Sensor})||Li system in operation in two different electrolytes: **a)** 1.2 M $LiPF_6$ in EC/EMC = 30/70 (v/v) and **b)** 1.0 M $LiPF_6$ in EC/DEC = 30/70 (v/v). In blue: potential profiles of LNMO (disordered) upon charging and discharging at C/10, and in black: charge at the platinum grid sensor biased at 1 V vs Li/Li$^+$ (chronoamperometry data can be found in the SI, Figs. S9a and c). (For interpretation of the references to color in this figure legend, the reader is referred to the Web version of this article.)

Table 1
Charge ratio at each operating stage of the LNMO electrode determined from the integrated charge on Fig. S10.

		$Mn^{3+/4+}$ (~4 V vs Li/Li$^+$)	$Ni^{2+/3+}$ (4.4–4.7 V)	$Ni^{3+/4+}$ (4.7–5V)
Q_{Sensor}/Q_{LNMO} (%)	1st Charge	0.36	0.78	0.71
	1st Discharge	0.23	0.36	0.34

efficiency" of 75 %, i.e. trapped/generated ratio of dissolved Mn. This ratio was calculated from the capacity extracted from the Mn and Pt electrodes, 9.6 mAh and 7.2 mAh respectively (see Fig. 2) considering a 2e-reaction $Mn^{+\ II}$ + 2e- ⇋ Mn (see Figs. S5 and S6) with no concomitant electrolyte reactions. The capacity associated to the reduction of the electrolyte only on the Pt mesh polarized at 1V vs Li/Li$^+$ can be indeed neglected as seen in Fig. S3. Note that the relatively large Pt mesh size tested here, i.e. ~300 µm (100 µm thick) may explain that a non-negligible part of soluble Mn is not captured by the sensor.

- Similar experiments were conducted using pure copper foils as positive electrode (Cu||(Pt_{Sensor})||Li cell), subjected to constant oxidative currents (+40, 80 µA, E_{ox} ≈ 3.5 V vs Li/Li$^+$, see Figs. S7a and c) and a Pt sensor polarized at 2V vs Li/Li$^+$ (see Figs. S7b and d). Capture efficiencies of 70 and 76 %, similar to those obtained with Mn, were obtained with Cu for the 40 and 80 µA dissolution currents respectively, suggesting that the capture efficiency is not affected by sensor polarization as long as it is within the electrolyte stability potential window.
- The generation of non-metal redox shuttles at a positive composite carbon electrode as reported in previous studies [40,41] was then evaluated on a C||(Pt_{Sensor})||Li cell in the same electrolyte composition. The C electrode was polarized such as to mimic the charging profile of the LNMO electrode (see SI). Reduction current could be detected on the Pt sensor (see Fig. S8), attesting of the reduction of species generated upon polarization of the cell. Only about 8 % of the charges consumed in electrolyte oxidation (Q_C = 18.7 µAh) are actually recovered on the Pt grid (Q_{Pt} = 1.5 µAh), suggesting that non-metallic redox shuttles are not produced at high rates and may not dominate the overall crosstalk process.

Since the sensing sensitivity does not appear to be system dependent and since the crosstalk of non-metallic species appears to be negligible compared to metallic species, a capture efficiency of 75 % will be considered in the following.

4 Influence of the electrode structure and the electrolyte composition

As the dissolution rate of Mn (convoluted by diffusion/migration) to the sensor seems to be prominent across the $Mn^{+\ III/+IV}$ oxidation step (higher current), a partially-ordered LNMO material with reduced $Mn^{+\ III}$ content was synthesized [52] (see Fig. S1), tested in the crosstalk sensing cell filled with EMC-based electrolyte and compared to disordered LNMO (see full description in SI). The similar current profiles registered at the Pt sensor and the similar dissolution rates observed for the two LNMO materials (see Fig. S12), despite the different capacities associated with the $Mn^{+\ III/+IV}$ reaction, rule out a dissolution mechanism based solely on $Mn^{+\ III}$ disproportionation (without oxidation of the electrolyte).

Since the dQ/dE analysis presented in Fig. 3 shows higher extent of metal leaching at higher potentials (>4.4 V) where electrolyte oxidation is expected to occur, and since mechanisms involving electrolyte oxidative degradation have been proposed previously to explain LNMO dissolution, the electrolyte composition is discussed hereafter. A crosstalk sensing experiment was carried out on the same LNMO||(Pt_{Sensor})||Li system in a second standard electrolyte mixture EC/DEC = 50/50 (v/v) 1.0 M $LiPF_6$, with supposedly lower resistance to electro-oxidation [53,54] than EC/EMC = 30/70 (v/v) 1.2 M $LiPF_6$ previously tested (see Fig. S10). The potential profiles extracted upon charging/discharging of LNMO/Li (5 cycles at C/10) in the two electrolyte compositions, the current and the charge measured at the Pt sensor are shown in Fig. 4a and b and Fig. S10.

Slightly distinct temporal profiles are observed for the two electrolyte compositions, particularly around the mid-charge where the relaxation of the sensor current to a plateau described earlier for in EMC-based electrolyte is traded for a gradual current increase in DEC-based electrolyte. Overall, the currents detected on the Pt sensor are clearly more intense in DEC-based electrolyte, resulting in a higher charge after 5 cycles (≈170 vs 100 µAh). Note that in both electrolytes the onset for current increase during the charge is observed around 4.2 V, which coincides with the $Mn^{+\ III}$ to $Mn^{+\ IV}$ transition in LNMO. Importantly, after cycling of the LNMO electrode in DEC-based electrolyte, Ni was also detected on the Pt sensor by XRF (see Fig. S14), in smaller amount though (55 µg vs 220 µg for Mn) but in line with the stoichiometry of the active material (Ni: 0.5, Mn: 1.5). The extent of Mn dissolution on operating composite LNMO electrodes and its contribution to the irreversible capacity loss of the LNMO/Li system, were estimated from the charge measured at the Pt sensor and at the LNMO electrode for the two electrolyte series (see full description in SI). The calculated Mn masses were confronted to those obtained by ex situ XRF on a fraction of the Pt mesh surface (0.78 cm^2), after disassembly of the cells. The results are

summarized in Table 2.

Despite significant differences, the values obtained by operando titration and ex situ XRF appear consistent, attesting of the relevance of the electrochemical titration method developed in this study. Over 5 charge/discharge cycles, higher amounts of dissolved/electrodeposited Mn can be inferred from the current intensity at the sensor in DEC as compared to EMC-based electrolyte. Mn dissolution, if directly related to the loss of active material (1.5 Mn lost for each "inactive" LNMO unit), represents 1 %–2 % of initial LNMO loading and 8–17 % of the total capacity loss depending on the electrolyte composition, which is consistent with the work of Dumaz et al. [15] reporting that the majority of the capacity lost on LNMO-based systems (LP30 electrolyte) could be attributed to electrolyte oxidation. The intricate relation between the electrolyte stability and the rate of dissolution of LNMO is further discussed in the following. A significant difference in the reactivity/degradation of DEC and EMC-based electrolytes has been already reported on LNMO electrodes at high potential (mass spectroscopy studies), with important gas formation above 4.7 V vs Li/Li^+ in EC-DEC $LiPF_6$ [55] and only minor decomposition of EC-EMC $LiPF_6$ electrolyte at potentials below 5 V[53]. The higher resistance to oxidation of EMC-based electrolytes (as compared to DEC-based ones) is confirmed by electrochemical measurements on non-reactive electrode material (gold) presented in Fig. S11. Potential threshold for oxidation of 4.2 and 4.6 V vs Li/Li^+ are observed for DEC and EMC-based electrolyte respectively, with currents about ten times the current measured in EC-EMC $LiPF_6$ at 4.6 V. The promoted dissolution of LNMO in contact with EC-DEC $LiPF_6$ together with the lower resistance to electro-oxidation of this electrolyte supports a dissolution mechanism of LNMO involving electrolyte oxidation intermediates already raised in previous studies [3,15,23] and a dissolution rate of LNMO modulated by the electrochemical stability of the electrolyte at high potential.

Performance of the sensing device – In the light of the obtained results, the performances of the proposed device are compared to that reported for various operando EPR and XAS studies.

- Sensitivity - From the calibration experiments on Mn/Li and Cu/Li systems, the threshold for detection of leached metal, above the current background noise, is estimated to be 0.32 mC, corresponding to 5.45 μmol or 0.27 ppm. Such sensitivity appears much higher than that reported for operando XAS [2] (i.e. noise level ≈0.25 mM for Mn^{2+} in NMC622/graphite cell cycled at C/2) or for operando EPR [3] (i.e. ≈15 ppm detection threshold for of Mn [2] in LNMO/Cu cycled at C/10). This high sensitivity of the device, makes it possible to detect charges on the sensor from the very first charge of LNMO (low amount of leached metal accumulated in the electrolyte), and at the different operating voltages of the LNMO (evidence of various leaching dynamics).
- Selectivity - If we are confident that metals can be selectively electrodeposited according to their redox potential, then all metals will be reduced at once at the lowest potential on the sensor. Each metal cannot therefore be selectively quantified in a single operando experiment as in XAS or EPR measurements.
- Quantification accuracy - The amount of metal leached at the end of the first charge on our system, i.e. 20.6 μAh, (74 mC, 3.2 mM and 210 ppm, or 4 mM, 260 ppm considering a 75 % capture efficiency) seems higher but in the same order of magnitude than that reported by operando EPR on LNMO/Cu (90 ppm for Mn^{2+}).
- Time resolution - The sampling rate of our device (based on current measurements only: ≈0.1s) is higher than for other reported operando techniques such as EPR (60s per scan [2]) or XAS (≈24 min per spectrum) [1], and should allow high C-rates to be tested. Note however that the sensor time response is convoluted by the transport of the redox shuttles in solution (≈60s delay between generation and collection)
- Finally, regarding the **relevance** of our analysis, the electrochemical footprint of our sensor on the tested system is minimal since our design is close that of real systems (electrode positioning, low flooding factors: 80 μL of electrolyte for 13 mm electrode diameter 13 mm and 7 mg/cm^2 AM loading), at least similar to that of operando XAS cells (2–4 glass separators >400 μm, 160 μL) as the cycling performances are similar to the one obtained on coin-cells [1].

4. Conclusion

The development of quantitative and integrated characterization techniques is seen as a major perspective research axis to monitor the so-called chemical crosstalk process and assess the effectiveness of remediation solutions. By intercalating an electrochemical sensor (a Pt mesh) with a minimal electrochemical "footprint" in a Li-battery cell (LNMO||(Pt_{Sensor})||Li), the effective detection and capture of redox-shuttles diffusing/migrating across a LNMO/Li cell could be demonstrated operando. This real-time crosstalk sensing technique (supported by ex situ chemical analysis of the sensor) allows dynamic quantification of the extent of metal dissolution from the positive electrode at each operating voltage of the electrode material (typically achieved by ex situ measurement on large volumes of electrolyte) and the correlation with the state of health of the electrode material. It therefore represents an affordable and complementary tool to advanced operando techniques such as XAS, EPR or NMR.

Our study revealed copious amounts of leached metal (Mn and Ni) at each operating voltage of the LNMO electrode (weigh percent loss of active material as high as 2 % after only 5 charging/discharging cycles), during both charge and discharge. The effective electroreduction/deposition and trapping of inter-crossing soluble Mn and Ni species is achieved at 1V on Pt, supporting their possible (disruptive) integration within the SEI developed at low voltage negative electrodes. Non-metallic redox shuttles could be also detected on the sensor but contribute in a much lesser extent to the overall crosstalk process than metallic species. The impact of the $Mn^{+\,III}$ content in two LNMO polymorphes on the dissolution rate and magnitude could not be evidenced, ruling out a dissolution mechanism based solely on disproportionation. However, an enhanced active material dissolution was demonstrated both in lesser oxidation resistant electrolyte and at Ni higher-operation voltage (as compared to Mn), confirming that electrolyte oxidation above 4.2 V may contribute directly or indirectly (electrolyte by-products) to the dissolution process.

The full analytical potential of the proposed crosstalk sensing technique could be unleashed through various optimizations steps including: **(i)** the exploration of various sensors characteristics and of new polarization strategies toward improved sensitivity (capture efficiency ~ 75 %

Table 2
Irreversible capacity of the LNMO||(Pt_{Sensor})||Li system associated to Mn leaching estimated from the sensor response ("operando titration") and from ex situ analyses (XRF on the Pt mesh) of the Pt sensor after 5 charge/discharge cycles of the LNMO electrode (disordered) at approximately C/10 and in two different electrolyte compositions (EMC & DEC-based electrolytes). The values in parenthesis account for the concomitant reduction of Ni(+II) in DEC-based electrolyte.

	Electrolyte composition	Mn mass on sensor (μg)	Equivalent inactive LNMO mass (μg)	% Inactive LNMO (weight)	% Total capacity loss
Operando "titration"	EC-EMC $LiPF_6$	105	234	1.15	14.2
	EC-DEC $LiPF_6$	177 (143)	393 (318)	1.67 (1.35)	13.9 (11.2)
Ex situ XRF	EC-EMC $LiPF_6$	63	139.8	0.68	8.5
	EC-DEC $LiPF_6$	220 + 55 (Ni)	489.2	2.08	17.3

at the moment) and selective capture and identification of the different redox-shuttles, **(ii)** the introduction of a reference electrode (4-electrode measurement) to explore different anode/cathode combinations and their impact on crosstalk phenomena, **(iii)** the assessment of ageing effects (long-term cycling, calendar aging at high-temperature), **(iv)** the precise identification of trapped redox-shuttles by cross-comparison with spectroscopic analyses of the sensor (e.g. surface-enhanced Raman SERS and mass-spectroscopy). The operando selective tracking and blocking of redox shuttles should facilitate the exploration of strategies [56] to mitigate metal leaching and shuttling, such as active material optimization (crystal shape, surface coatings) and electrode structuring, electrolyte additives [57], optimized and/or appropriate separator design for cross-talk shielding [29,58] and could be applied to other battery chemistries including Li-air and Li-sulfur batteries.

CRediT authorship contribution statement

Antonin Gajan: Writing – review & editing, Writing – original draft, Supervision, Methodology, Investigation, Formal analysis, Data curation, Conceptualization. **Kethsovann Var:** Methodology, Investigation, Formal analysis, Data curation. **Rajmohan Rajendiran:** Investigation, Data curation. **Jean-François Lemineur:** Writing – review & editing, Methodology, Investigation. **Olivier Guiader:** Writing – review & editing, Investigation, Conceptualization. **Benoit Mortemard de Boisse:** Writing – review & editing, Formal analysis, Conceptualization. **Bernard Simon:** Investigation, Conceptualization. **Julien Demeaux:** Writing – review & editing, Supervision, Project administration, Investigation, Funding acquisition, Conceptualization. **Ivan T. Lucas:** Writing – review & editing, Writing – original draft, Visualization, Validation, Supervision, Resources, Project administration, Methodology, Investigation, Funding acquisition, Formal analysis, Data curation, Conceptualization.

Associated content

The Supporting information includes extra experimental details and 15 figures covering: i) the LNMO polymorphs preparation, characterization and performance, ii) the crosstalk sensing method description, iii) the assessment of the crosstalk sense cell performance, iv) the assessment of Mn leaching upon cycling of LNMO (detailed calculation), v) the oxidation threshold of carbonate based electrolyte, vi) the influence of the crystal structure of LNMO on its dissolution, vii) the XRF analyses of the Pt sensor.

Funding sources

This project was funded by the battery manufacturer Saft (a company of TotalEnergies), the ANRT (CIFRE n°2018/1579), by the ANR-CarLIB (grant numbers: ANR-15-CE05-0002), by the European Union's Horizon Europe research and innovation program (OPINCHARGE project, grant agreement ID:101104032). I.T.L. acknowledges Battery2030+.

Declaration of competing interest

The authors declare that they have no known competing financial interests or personal relationships that could have appeared to influence the work reported in this paper.

Acknowledgment

We would like to thank F. Pillier at LISE laboratory for the electron microscopy analyses.

Appendix A. Supplementary data

Supplementary data to this article can be found online at https://doi.org/10.1016/j.jpowsour.2024.236031.

Data availability

Data will be made available on request.

References

[1] J. Wandt, A. Freiberg, R. Thomas, Y. Gorlin, A. Siebel, R. Jung, H.A. Gasteiger, M. Tromp, Transition metal dissolution and deposition in Li-ion batteries investigated by operando X-ray absorption spectroscopy, J. Mater. Chem. A 4 (47) (2016) 18300–18305, https://doi.org/10.1039/c6ta08865a.

[2] R. Jung, F. Linsenmann, R. Thomas, J. Wandt, S. Solchenbach, F. Maglia, C. Stinner, M. Tromp, H.A. Gasteiger, Nickel, manganese, and cobalt dissolution from Ni-rich NMC and their effects on nmc622-graphite cells, J. Electrochem. Soc. 166 (2) (2019) A378–A389, https://doi.org/10.1149/2.1151902jes.

[3] J.C. Hestenes, J.T. Sadowski, R. May, L.E. Marbella, Transition metal dissolution mechanisms and impacts on electronic conductivity in composite LiNi0.5Mn1.5O4 cathode films, ACS Mater. Au 3 (2) (2022) 88–101, https://doi.org/10.1021/acsmaterialsau.2c00060.

[4] Y. Xia, Y. Zhou, M. Yoshio, Capacity fading on cycling of 4 V Li/LiMn2 O 4 cells, J. Electrochem. Soc. 144 (8) (1997) 2593, https://doi.org/10.1149/1.1837870.

[5] H. Yang, G.V. Zhuang, P.N. Ross, Thermal stability of LiPF6 salt and Li-ion battery electrolytes containing LiPF6, J. Power Sources 161 (1) (2006) 573–579, https://doi.org/10.1016/j.jpowsour.2006.03.058.

[6] D.P. Abraham, T. Spila, M.M. Furczon, E. Sammann, Evidence of transition-metal accumulation on aged graphite anodes by SIMS, Electrochem. Solid State Lett. 11 (12) (2008) A226, https://doi.org/10.1149/1.2987680.

[7] H. Zheng, Q. Sun, G. Liu, X. Song, V.S. Battaglia, Correlation between dissolution behavior and electrochemical cycling performance for LiNi1/3Co1/3Mn1/3O2-based cells, J. Power Sources 207 (2012) 134–140, https://doi.org/10.1016/j.jpowsour.2012.01.122.

[8] D.R. Gallus, R. Schmitz, R. Wagner, B. Hoffmann, S. Nowak, I. Cekic-Laskovic, R. W. Schmitz, M. Winter, The influence of different conducting salts on the metal dissolution and capacity fading of NCM cathode material, Electrochim. Acta 134 (2014) 393–398, https://doi.org/10.1016/j.electacta.2014.04.091.

[9] X. Liao, Q. Huang, S. Mai, X. Wang, M. Xu, L. Xing, Y. Liao, W. Li, Understanding self-discharge mechanism of layered nickel cobalt manganese oxide at high potential, J. Power Sources 286 (2015) 551–556, https://doi.org/10.1016/j.jpowsour.2015.04.032.

[10] I. Buchberger, S. Seidlmayer, A. Pokharel, M. Piana, J. Hattendorff, P. Kudejova, R. Gilles, H.A. Gasteiger, Aging analysis of graphite/$LiNi_{1/3}Mn_{1/3}Co_{1/3}O_2$ cells using XRD, PGAA, and AC impedance, J. Electrochem. Soc. 162 (14) (2015) A2737–A2746, https://doi.org/10.1149/2.0721514jes.

[11] J.A. Gilbert, I.A. Shkrob, D.P. Abraham, Transition metal dissolution, ion migration, electrocatalytic reduction and capacity loss in lithium-ion full cells, J. Electrochem. Soc. 164 (2) (2017) A389–A399, https://doi.org/10.1149/2.1111702jes.

[12] D.H. Jang, Y.J. Shin, S.M. Oh, Dissolution of spinel oxides and capacity losses in 4 V $Li/Li_xMn_2O_4$ cells, J. Electrochem. Soc. 143 (7) (1996) 2204, https://doi.org/10.1149/1.1836981.

[13] R. Jung, M. Metzger, F. Maglia, C. Stinner, H.A. Gasteiger, Chemical versus electrochemical electrolyte oxidation on NMC111, NMC622, NMC811, LNMO, and conductive carbon, J. Phys. Chem. Lett. 8 (19) (2017) 4820–4825, https://doi.org/10.1021/acs.jpclett.7b01927.

[14] B.L.D. Rinkel, D.S. Hall, I. Temprano, C.P. Grey, Electrolyte oxidation pathways in lithium-ion batteries, J. Am. Chem. Soc. 142 (35) (2020) 15058–15074, https://doi.org/10.1021/jacs.0c06363.

[15] P. Dumaz, C. Rossignol, A. Mantoux, N. Sergent, R. Bouchet, Kinetics analysis of the electro-catalyzed degradation of high potential LiNi0,5Mn1,5O4 active materials, J. Power Sources 469 (2020) 228337, https://doi.org/10.1016/j.jpowsour.2020.228337.

[16] J.M. Tarascon, W.R. McKinnon, F. Coowar, T.N. Bowmer, G. Amatucci, D. Guyomard, Synthesis conditions and oxygen stoichiometry effects on Li insertion into the spinel LiMn2 O 4, J. Electrochem. Soc. 141 (6) (1994) 1421, https://doi.org/10.1149/1.2054941.

[17] M. Ochida, Y. Domi, T. Doi, S. Tsubouchi, H. Nakagawa, T. Yamanaka, T. Abe, Z. Ogumi, Influence of manganese dissolution on the degradation of surface films on edge plane graphite negative-electrodes in lithium-ion batteries, J. Electrochem. Soc. 159 (7) (2012) A961–A966, https://doi.org/10.1149/2.031207jes.

[18] C. Delacourt, A. Kwong, X. Liu, R. Qiao, W.L. Yang, P. Lu, S.J. Harris, V. Srinivasan, Effect of manganese contamination on the solid-electrolyte-interphase properties in Li-ion batteries, J. Electrochem. Soc. 160 (8) (2013) A1099–A1107, https://doi.org/10.1149/2.035308jes.

[19] N.P.W. Pieczonka, Z. Liu, P. Lu, K.L. Olson, J. Moote, B.R. Powell, J.-H. Kim, Understanding transition-metal dissolution behavior in LiNi0.5Mn1.5O4 high-voltage spinel for lithium ion batteries, J. Phys. Chem. C 117 (31) (2013) 15947–15957, https://doi.org/10.1021/jp405158m.

[20] C. Zhan, J. Lu, A. Jeremy Kropf, T. Wu, A.N. Jansen, Y.K. Sun, X. Qiu, K. Amine, Mn (II) deposition on anodes and its effects on capacity fade in spinel lithium manganate-carbon systems, Nat. Commun. 4 (2013) 2437, https://doi.org/10.1038/ncomms3437.

[21] S.R. Gowda, K.G. Gallagher, J.R. Croy, M. Bettge, M.M. Thackeray, M. Balasubramanian, Oxidation state of cross-over manganese species on the

graphite electrode of lithium-ion cells, Phys. Chem. Chem. Phys. 16 (15) (2014) 6898–6902, https://doi.org/10.1039/c4cp00764f.
[22] L. Madec, R. Petibon, K. Tasaki, J. Xia, J.P. Sun, I.G. Hill, J.R. Dahn, Mechanism of action of ethylene sulfite and vinylene carbonate electrolyte additives in LiNi1/3Mn1/3Co1/3O2/graphite pouch cells: electrochemical, GC-MS and XPS analysis, Phys. Chem. Chem. Phys. 17 (40) (2015) 27062–27076, https://doi.org/10.1039/c5cp04221f.
[23] A. Jarry, S. Gottis, Y.S. Yu, J. Roque-Rosell, C. Kim, J. Cabana, J. Kerr, R. Kostecki, The formation mechanism of fluorescent metal complexes at the Li(x)Ni(0.5)Mn(1.5)O(4-delta)/carbonate ester electrolyte interface, J. Am. Chem. Soc. 137 (10) (2015) 3533–3539, https://doi.org/10.1021/ja5116698.
[24] M. Evertz, F. Horsthemke, J. Kasnatscheew, M. Börner, M. Winter, S. Nowak, Unraveling transition metal dissolution of $Li_{1.04}Ni_{1/3}Co_{1/3}Mn_{1/3}O_2$ (NCM 111) in lithium ion full cells by using the total reflection X-ray fluorescence technique, J. Power Sources 329 (2016) 364–371, https://doi.org/10.1016/j.jpowsour.2016.08.099.
[25] S. Solchenbach, G. Hong, A.T.S. Freiberg, R. Jung, H.A. Gasteiger, Electrolyte and SEI decomposition reactions of transition metal ions investigated by on-line electrochemical mass spectrometry, J. Electrochem. Soc. 165 (14) (2018) A3304–A3312, https://doi.org/10.1149/2.0511814jes.
[26] M.-T.F. Rodrigues, K. Kalaga, S.E. Trask, I.A. Shkrob, D.P. Abraham, Anode-dependent impedance rise in layered-oxide cathodes of lithium-ion cells, J. Electrochem. Soc. 165 (9) (2018) A1697–A1705, https://doi.org/10.1149/2.0611809jes.
[27] D. Leanza, C.A.F. Vaz, G. Melinte, X. Mu, P. Novak, M. El Kazzi, Revealing the dual surface reactions on a HE-NCM Li-ion battery cathode and their impact on the surface chemistry of the counter electrode, Appl. Mater. Interfaces 11 (6) (2019) 6054–6065, https://doi.org/10.1021/acsami.8b19511.
[28] T. Joshi, K. Eom, G. Yushin, T.F. Fuller, Effects of dissolved transition metals on the electrochemical performance and SEI growth in lithium-ion batteries, J. Electrochem. Soc. 161 (12) (2014) A1915–A1921, https://doi.org/10.1149/2.0861412jes.
[29] R. Sahore, F. Dogan, I.D. Bloom, Identification of electrolyte-soluble organic cross-talk species in a lithium-ion battery via a two-compartment cell, Chem. Mater. 31 (8) (2019) 2884–2891, https://doi.org/10.1021/acs.chemmater.9b00063.
[30] C.P. Aiken, J. Self, R. Petibon, X. Xia, J.M. Paulsen, J.R. Dahn, A survey of in situ gas evolution during high voltage formation in Li-ion pouch cells, J. Electrochem. Soc. 162 (4) (2015) A760–A767, https://doi.org/10.1149/2.0941504jes.
[31] C.P. Aiken, J. Xia, D.Y. Wang, D.A. Stevens, S. Trussler, J.R. Dahn, An apparatus for the study of in situ gas evolution in Li-ion pouch cells, J. Electrochem. Soc. 161 (10) (2014) A1548–A1554, https://doi.org/10.1149/2.0151410jes.
[32] C. Bolli, A. Guéguen, M.A. Mendez, E.J. Berg, Operando monitoring of F–formation in lithium ion batteries, Chem. Mater. 31 (4) (2019) 1258–1267, https://doi.org/10.1021/acs.chemmater.8b03810.
[33] G. Yan, D. Alves-Dalla-Corte, W. Yin, N. Madern, G. Gachot, J.-M. Tarascon, Assessment of the electrochemical stability of carbonate-based electrolytes in Na-ion batteries, J. Electrochem. Soc. 165 (7) (2018) A1222–A1230, https://doi.org/10.1149/2.0311807jes.
[34] N.S. Norberg, S.F. Lux, R. Kostecki, Interfacial side-reactions at a LiNi0.5Mn1.5O4 electrode in organic carbonate-based electrolytes, Electrochem. Commun. 34 (2013) 29–32, https://doi.org/10.1016/j.elecom.2013.04.007.
[35] Y. Qiao, Z. Zhou, Z. Chen, S. Du, Q. Cheng, H. Zhai, N.J. Fritz, Q. Du, Y. Yang, Visualizing ion diffusion in battery systems by fluorescence microscopy: a case study on the dissolution of LiMn2O4, Nano Energy 45 (2018) 68–74, https://doi.org/10.1016/j.nanoen.2017.12.036.
[36] L.-F. Wang, C.-C. Ou, K.A. Striebel, J.-S. Chen, Study of Mn dissolution from $LiMn_2O_4$ spinel electrodes using rotating ring-disk collection experiments, J. Electrochem. Soc. 150 (7) (2003) A905, https://doi.org/10.1149/1.1577543.
[37] G.A. Snook, T.D. Huynh, A.F. Hollenkamp, A.S. Best, Rapid SECM probing of dissolution of LiCoO2 battery materials in an ionic liquid, J. Electroanal. Chem. 687 (2012) 30–34, https://doi.org/10.1016/j.jelechem.2012.08.021.
[38] J.C. Hunter, Preparation of a new crystal form of manganese dioxide: λ-MnO2, J. Solid State Chem. 39 (2) (1981) 142–147, https://doi.org/10.1016/0022-4596(81)90323-6.
[39] V. Meunier, M. Leal De Souza, M. Morcrette, A. Grimaud, Design of workflows for crosstalk detection and lifetime deviation onset in Li-ion batteries, Joule 7 (1) (2023) 42–56, https://doi.org/10.1016/j.joule.2022.12.004.
[40] J.A. Read, A.V. Cresce, M.H. Ervin, K. Xu, Dual-graphite chemistry enabled by a high voltage electrolyte, Energy Environ. Sci. 7 (2) (2014) 617–620, https://doi.org/10.1039/c3ee43333a.
[41] K. Ariyoshi, A. Maekawa, T. Nakamura, Quantification analysis and kinetic modeling of crosstalk reactions in lithium-ion batteries using a four-electrode cell, J. Electroanal. Chem. 916 (2022) 116383, https://doi.org/10.1016/j.jelechem.2022.116383.
[42] M.M. Thackeray, P.J. Johnson, L.A. de Picciotto, P.G. Bruce, J.B. Goodenough, Electrochemical extraction of lithium from LiMn2O4, Mater. Res. Bull. 19 (2) (1984) 179–187, https://doi.org/10.1016/0025-5408(84)90088-6.
[43] D. Tang, Y. Sun, Z. Yang, L. Ben, L. Gu, X. Huang, Surface structure evolution of LiMn2O4 cathode material upon charge/discharge, Chem. Mater. 26 (11) (2014) 3535–3543, https://doi.org/10.1021/cm501125e.
[44] A. Banerjee, Y. Shilina, B. Ziv, J.M. Ziegelbauer, S. Luski, D. Aurbach, I.C. Halalay, On the oxidation state of manganese ions in Li-ion battery electrolyte solutions, J. Am. Chem. Soc. 139 (5) (2017) 1738–1741, https://doi.org/10.1021/jacs.6b10781.
[45] R. Qiao, Y. Wang, P. Olalde-Velasco, H. Li, Y.-S. Hu, W. Yang, Direct evidence of gradient Mn(II) evolution at charged states in LiNi0.5Mn1.5O4 electrodes with capacity fading, J. Power Sources 273 (2015) 1120–1126.
[46] I.A. Shkrob, A.J. Kropf, T.W. Marin, Y. Li, O.G. Poluektov, J. Niklas, D.P. Abraham, Manganese in graphite anode and capacity fade in Li ion batteries, J. Phys. Chem. C 118 (42) (2014) 24335–24348, https://doi.org/10.1021/jp507833u.
[47] A. Blyr, A. Du Pasquier, G. Amatucci, J.M. Tarascon, Origin of self-discharge mechanism in LiMn2O4-based Li-ion cells: a chemical and electrochemical approach, Ionics 3 (5–6) (1997) 321–331, https://doi.org/10.1007/bf02375706.
[48] G.G. Amatucci, C.N. Schmutz, A. Blyr, C. Sigala, A.S. Gozdz, D. Larcher, J. M. Tarascon, Materials' effects on the elevated and room temperature performance of CLiMn2O4 Li-ion batteries, J. Power Sources 69 (1997) 11–25, https://doi.org/10.1016/S0378-7753(97)02542-1.
[49] D. Aurbach, M.D. Levi, K. Gamulski, B. Markovsky, G. Salitra, E. Levi, U. Heider, L. Heider, R. Oesten, Capacity fading of LixMn2O4 spinel electrodes studied by XRD and electroanalytical techniques, J. Power Sources 81–82 (1999) 472–479, https://doi.org/10.1016/S0378-7753(99)00204-9.
[50] B. Aktekin, M.J. Lacey, T. Nordh, R. Younesi, C. Tengstedt, W. Zipprich, D. Brandell, K. Edström, Understanding the capacity loss in LiNi0.5Mn1.5O4–Li4Ti5O12 lithium-ion cells at ambient and elevated temperatures, J. Phys. Chem. C 122 (21) (2018) 11234–11248, https://doi.org/10.1021/acs.jpcc.8b02204.
[51] B. Liao, H. Li, M. Xu, L. Xing, Y. Liao, X. Ren, W. Fan, L. Yu, K. Xu, W. Li, Designing low impedance interface films simultaneously on anode and cathode for high energy batteries, Adv. Energy Mater. 8 (22) (2018) 1800802, https://doi.org/10.1002/aenm.201800802.
[52] L. Wang, H. Li, X. Huang, E. Baudrin, A comparative study of Fd-3m and P4332 "LiNi0.5Mn1.5O4", Solid State Ionics 193 (1) (2011) 32–38, https://doi.org/10.1016/j.ssi.2011.04.007.
[53] W. Weber, R. Wagner, B. Streipert, V. Kraft, M. Winter, S. Nowak, Ion and gas chromatography mass spectrometry investigations of organophosphates in lithium ion battery electrolytes by electrochemical aging at elevated cathode potentials, J. Power Sources 306 (2016) 193–199, https://doi.org/10.1016/j.jpowsour.2015.12.025.
[54] C. Wang, L. Xing, J. Vatamanu, Z. Chen, G. Lan, W. Li, K. Xu, Overlooked electrolyte destabilization by manganese (II) in lithium-ion batteries, Nat. Commun. 10 (1) (2019) 3423, https://doi.org/10.1038/s41467-019-11439-8.
[55] H. Wang, E. Rus, T. Sakuraba, J. Kikuchi, Y. Kiya, H.D. Abruña, CO2 and O2 evolution at high voltage cathode materials of Li-ion batteries: a differential electrochemical mass spectrometry study, Anal. Chem. 86 (13) (2014) 6197–6201, https://doi.org/10.1021/ac403317d.
[56] Y. Song, L. Wang, L. Sheng, D. Ren, H. Liang, Y. Li, A. Wang, H. Zhang, H. Xu, X. He, The significance of mitigating crosstalk in lithium-ion batteries: a review, Energy Environ. Sci. 16 (5) (2023) 1943–1963, https://doi.org/10.1039/d3ee00441d.
[57] S. Klein, L. Haneke, P. Harte, L. Stolz, S. van Wickeren, K. Borzutzki, S. Nowak, M. Winter, T. Placke, J. Kasnatscheew, Suppressing electrode crosstalk and prolonging cycle life in high-voltage Li ion batteries: pivotal role of fluorophosphates in electrolytes, Chemelectrochem 9 (13) (2022) e202200469, https://doi.org/10.1002/celc.202200469.
[58] X.-Q. Zhang, X.-M. Wang, B.-Q. Li, P. Shi, J.-Q. Huang, A. Chen, Q. Zhang, Crosstalk shielding of transition metal ions for long cycling lithium–metal batteries, J. Mater. Chem. A 8 (8) (2020) 4283–4289, https://doi.org/10.1039/c9ta12269a.